AIChE

Theoretical Analysis of the Effects of Asymmetric Membrane Structure on Fouling During Microfiltration

Weiyi Li
Dept. of Chemical and Materials Engineering, University of Cincinnati, Cincinnati, OH 45221

Chase Duclos-Orsello
Millipore Corporation, Bedford, MA 01730

Chia-Chi Ho
Dept. of Chemical and Materials Engineering, University of Cincinnati, Cincinnati, OH 45221

DOI 10.1002/aic.11763
Published online May 5, 2009 in Wiley InterScience (www.interscience.wiley.com).

There is a growing interest in the use of both asymmetric and composite membranes for microfiltration and ultrafiltration processes. This includes particle removal applications in the semiconductor industry and virus clearance in biopharmaceutical applications. Filter fouling plays an important role in these processes. Although flux decline models have been developed for homogeneous membranes, the effects of asymmetric membrane structure on flux decline behavior remain poorly understood on a fundamental level. Here, we develop a theoretical model to describe the effects of asymmetric membrane structure on flux decline. The asymmetric structure was described by the spatial variation in Darcy permeability in the directions normal to and parallel to the membrane surface. The velocity profile and flux decline because of pore blockage were described using Darcy's law and a pore blockage and cake filtration model. Flux decline data were obtained using pseudocomposite membranes with highly interconnected polyvinylidene fluoride membranes (PVDF) and straight through pore polycarbonate track-etched membranes (PCTE). Model composite membranes were formed by layering PCTE or PVDF membranes with different pore sizes on top of each other. Flux decline data for the composite membrane were in good agreement with model calculations. The results provide important insights into the effects of asymmetric membrane pore structures on flux decline. © 2009 American Institute of Chemical Engineers *AIChE J,* 55: 1434–1446, 2009

Keywords: asymmetric pore structures, microfiltration, membrane fouling, pore connectivity

Introduction

Microfiltration membranes are widely used in the dairy and biotechnology industries. Biofouling is often encountered during the microfiltration processes. Many fouling models have been developed to describe flux decline during

Correspondence concerning this article should be addressed to C.-C. Ho at cho@alpha.che.uc.edu

filtration by assuming a particular fouling mechanism. These include: the complete pore blockage model, the intermediate pore blockage model, the cake filtration model, and the pore constriction model.[1–3] Recently, it has been identified that the combining of these models leads to better agreement with fouling data.[4–6] Most previous models assumed that the membranes had symmetric structures, or were composed of an array of straight through cylindrical pores.

Traditionally, commercial microfiltration membranes have had homogeneous structures; however, there is increasing use of asymmetric and composite membranes. Ho and Zydney[7,8] developed a mathematical model accounting for the effects of the membrane morphology on the fouling processes. The pore interconnectivity can be mathematically described by the ratio of the permeability in the radial direction to that in the transverse direction, and this permeability ratio can be determined by experiments.[9] Jackson et al.[10] also related the membrane structure to transport phenomena in an effort to improve the understanding of the microfiltration or ultrafiltration processes by using a stochastic model to describe the pore geometric properties. Although all these models accounted for the lateral flow within the membrane structure, the membranes were treated as homogeneous porous structures.

In contrast to symmetric membranes, asymmetric membranes usually have a very thin skin layer that determines the membrane selectivity and a relatively thick porous supporting layer.[11] Asymmetric membranes can have better performance than the symmetric membranes because the retentive layer in an asymmetric membrane can be thinner, thereby reducing the membrane resistance relative to a symmetric membrane of similar retentive capability. Highly asymmetric membranes with pores that gradually decrease in size from the feed side to the permeate side and membranes having layers of different porosity also have been manufactured.[12–15] Although various techniques for making asymmetric membranes are now available, it is not clearly understood on a fundamental level how the structure of asymmetric membranes affects the flux decline behavior during filtration. Ho and Zydney[16,17] developed a mathematical model explicitly accounting for fluid flow through composite membranes formed with two layers: an upper layer with noninterconnected pores and substructure with highly interconnected pores. However, the pore connectivity in this model cannot be varied. Thus, it is difficult to apply this model to describe membranes with varying degree of pore connectivity throughout the membrane.

The objective of this study was to develop a mathematical description of flux decline behavior for membranes with different asymmetric structures. The asymmetric structure is characterized by the radial and axial permeabilities within the membrane, which were varied in the transverse direction to simulate composite membranes. The model predictions were then compared with the experimental flux decline data during dead end filtration of polystyrene microsphere solutions and bovine serum albumin (BSA) solutions through membranes composed of two layers with different pore connectivities.

Theory

We assume that fouling occurs through the pore blockage mechanism with the particles depositing uniformly and randomly over the membrane surface. At low surface coverage, the flow through the membrane can be described by a Krogh-cylinder-type model,[18] which assumes that the foulants deposit at the center of the characteristic region, whereas the fluid flows around the blocked area (as shown in the left panel of Figure 1). As the membrane becomes more highly fouled, the fluid will flow primarily through a hole that is surrounded by foulants (as shown in the right panel of Figure 1). The radius of the Krogh cylinder is determined by fraction of surface coverage θ. For the case of central blockage, the fraction of blocked area θ can be calculated by:

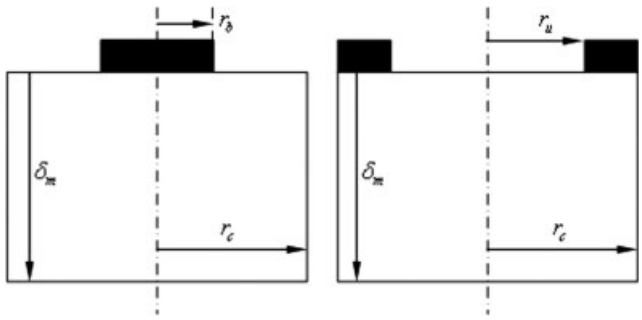

Figure 1. Schematic of the top surface of a partially fouled membrane showing the Krogh cylinder approximation with central blockage (left panel) and central void (right panel).

$$\theta = \left(\frac{r_b}{r_c}\right)^2. \tag{1}$$

For the case of central void, it can be expressed by:

$$\theta = 1 - \left(\frac{r_u}{r_c}\right)^2. \tag{2}$$

The local pressure within the membrane structures can be obtained by combining Darcy's Law and the continuity equation.

$$\frac{1}{r}\frac{\partial}{\partial r}\left(rk_r\frac{\partial p}{\partial r}\right) + \frac{\partial}{\partial z}\left(k_z\frac{\partial p}{\partial z}\right) = 0, \tag{3}$$

where k_r and k_z are the Darcy permeabilities in the radial and transverse directions, respectively. Membranes with straight through pores were modeled with $\frac{k_r}{k_z} = 0$, whereas those with interconnected pores had $\frac{k_r}{k_z} = 1$. In earlier studies,[8,9] a constant permeability ratio of k_r to k_z was used to describe the symmetric membrane structures. For asymmetric membrane structures, the permeabilities are functions of the location in the transverse direction. The boundary conditions can be expressed as:

$$\frac{\partial p}{\partial r} = 0 \qquad at\ r = 0 \tag{4}$$

$$\frac{\partial p}{\partial r} = 0 \qquad at\ r = r_c \tag{5}$$

$$\begin{cases} \dfrac{p_f - p}{\mu R_p} = -k_z \dfrac{\partial p}{\partial z}\Big|_{z=0} & 0 \le r \le r_b \\ & at\ z = 0 \\ p = p_f & r_b < r \le r_c \end{cases} \quad (6)$$

$$p = p_p \qquad at\ z = \delta_m \quad (7)$$

where r_b and r_c are the radius for the blocked area and the entire characteristic region, respectively, δ_m is the thickness of membrane, p_f and p_p are the pressures of feed and permeate, respectively, and R_p is the resistance of the fouling layer. For the central void case (Figure 1b), the corresponding boundary condition at $z = 0$ should be written as:

$$\begin{cases} p = p_f & 0 < r \le r_u \\ & at\ z = 0 \\ \dfrac{p_f - p}{\mu R_p} = -k_z \dfrac{\partial p}{\partial z}\Big|_{z=0} & r_u \le r \le r_c \end{cases} \quad (8)$$

where r_u is the radius of the central open area.

For the asymmetric structure, both k_r and k_z are a function of the position in transverse direction. We normalize the governing equation to give:

$$\frac{1}{r^*}\frac{\partial}{\partial r^*}\left(r^* K_z K \frac{\partial p^*}{\partial r^*}\right) + \frac{\partial}{\partial z^*}\left(K_z \frac{\partial p^*}{\partial z^*}\right) = 0, \quad (9)$$

where $r^* = \frac{r}{r_b}$, $z^* = \frac{z}{\delta_m}$, $p^* \frac{p - p_p}{p_f - p_p}$. K_z is the dimensionless permeability in the transverse direction:

$$K_z(z^*) = \frac{k_z}{k_z|_{z=0}} \quad (10)$$

This parameter characterizes the variation of the membrane resistance. K is the normalized permeability ratio:

$$K(z^*) = \left(\frac{\delta_m}{r_b}\right)^2 \frac{k_r}{k_z}, \quad (11)$$

which characterizes the variation of the pore connectivity.

To calculate the total filtrate flux as a function of time, the governing equation Eq. 3 needs to be combined with an external fouling model to determine the relationship between the fraction of blocked area and filtration time. Here, we use the combined pore blockage and cake filtration model developed by Ho and Zydney.[4] In this model, the rate for pore blockage and cake filtration can be obtained by the convective transport of foulant to the specific regions. The rate of blockage has been assumed to be proportional to the convective flow rate of foulants to the membrane surface:

$$\frac{dA_u}{dt} = -\alpha J_u A_u C_b, \quad (12)$$

where α is the area of covered membrane per unit mass of foulant. It is a function of particle size r_p, membrane pore size r_m, and membrane porosity ε_m[7]:

$$\alpha = \frac{1}{\varepsilon_m}\left(\frac{r_m}{r_p}\right)^2 \alpha'. \quad (13)$$

As the parameter α' is the projected area of particles per unit mass of foulant, it is independent of the properties of membrane.

The hydraulic resistance of the fouling layer is assumed to be proportional to the convective transport of foulants through the blocked area:

$$\frac{dR_p}{dt} = f' R' J_b C_b, \quad (14)$$

where f' is the fraction of the particles contributing to the growth of the deposit, and R' is the specific cake layer resistance, which is assumed to be constant during a constant pressure filtration. Although the cake layer would be spatially inhomogeneous because of the time dependent blockage of the membrane surface,[4] here we assumed that the cake layer is spatially uniform. This assumption is valid because cake growth is a self-leveling process.[4] Previous studies[19] showed that R' was a function of the transmembrane pressure because of the compressibility of the protein deposit:

$$R' = k_p\left(\frac{\Delta p}{1N/m^2}\right)^S, \quad (15)$$

where the compressibility parameter S varies from 0 for an incompressible cake to 1 for a very highly compressible cake layer.

Both J_u and J_b are a function of the fraction of blocked area θ and the resistance of the cake layer within the blocked area. They can be calculated by integrating the pressure gradient at the corresponding area on the membrane surface. For the central blockage case, they can be expressed as:

$$J_b = \frac{2\pi \int_0^{r_b} -k_z \frac{\partial p}{\partial z}\big|_{z=0} r dr}{\theta \pi r_c^2} \quad (16)$$

$$J_u = \frac{2\pi \int_{r_b}^{r_c} -k_z \frac{\partial p}{\partial z}\Big|_{z=0} r dr}{(1-\theta)\pi r_c^2}. \quad (17)$$

For the central void case, they can be expressed as:

$$J_b = \frac{2\pi \int_{r_u}^{r_c} -k_z \frac{\partial p}{\partial z}\big|_{z=0} r dr}{\theta \pi r_c^2} \quad (18)$$

$$J_u = \frac{2\pi \int_0^{r_u} -k_z \frac{\partial p}{\partial z}\big|_{z=0} r dr}{(1-\theta)\pi r_c^2}. \quad (19)$$

The total filtration flux can be obtained by combining Eqs. 3, 12, and 14 with the flux determined using Eqs. 16–19. Equation 3 can be numerically solved by the method of finite element, and Eqs. 12 and 14 can be numerically solved by the second-order Runge-Kutta method.[20]

Materials and Methods

Materials

The 0.25-μm polystyrene microspheres (catalog number PSO2N/5935) were purchased from Bangs Laboratories

(Fishers, IN) and prepared by diluting different concentrations of polystyrene microspheres in deionized (DI) water. BSA solutions were prepared by dissolving BSA powder (initial fractionation by heat shock, catalog number A7906, Sigma) in the desired volume of DI water. All BSA solutions were freshly prepared before each experiment and used within 8 h of preparation.

The membranes used for flux decline measurements were as follows: 0.2 μm polycarbonate track-etched membranes (PCTE, filter code GTTP, Millipore) and hydrophilic Durapore® microfiltration membranes with nominal pore size ratings of 0.1 μm (polyvinylidene fluoride (PVDF), filter code VVLP, Millipore), 0.22 μm (PVDF, filter code GVWP, Millipore), and 0.45 μm (PVDF, filter code HVLP, Millipore).

Filtration experiments

All dead end filtrations were performed under constant pressure conditions in a 25 mm diameter ultrafiltration cell (Model 8010, Amicon Co., Beverly, MA) connected to an acrylic solution reservoir. The transmembrane pressure was provided by compressed air. Pressures ranging from 2 to 12 psi were used to limit the initial filtrate flow within a certain value. The filtrate flow rate was measured by a digital balance (PB3002-S, DeltaRange, Mettler Toledo) and automatically recorded by measurement software BalanceTalk (Version 4.0, Labtronics). All experiments were performed at room temperature (20°C).

Polystyrene microsphere solutions with concentration varying from 0.00125 to 0.01 g/L were used to filter through polycarbonate track-etched membranes, hydrophilic Durapore membranes, and double-layer membranes. BSA solutions with concentration varying from 1 to 4 g/L were used to filter through polycarbonate track-etched membranes, hydrophilic Durapore membranes, and the same double-layer membranes combinations. All membranes were compressed using a pressure 1.5 times higher than the filtration pressure for 30 min before the flux decline measurements to minimize the effects of membrane compaction.

Before the flux decline measurements, all membranes were tested with pure DI water to obtain the permeability in the transverse direction k_z. The DI water permeate flux was measured at different transmembrane pressures (from 0 to 12 psi), and transverse permeability was obtained by:

$$J = k_z \frac{\Delta p}{\delta_m}. \tag{20}$$

In particular, for the double-layer membranes, the hydraulic permeability for both layers was recorded before and after the flux decline measurements.

To fit the compressibility parameter S, 0.2 μm PCTE membranes were fouled by 0.00125 g/L polystyrene beads or 1 g/L BSA for 2 h. Then, these fouled membranes were used to measure the permeability under transmembrane pressures varying from 2 to 12 psi.

Theoretical Results

Model simulation

The model accounting for the effect of membrane morphology was used to simulate the composite membranes with asymmetric structures. The distribution of normalized pressure was calculated by solving the governing equation by finite element analysis, and the streamlines can be obtained directly in terms of the distribution of velocities determined by the pressure gradient:

$$\psi = \int r(u_z dr - u_r dz), \tag{21}$$

where $u_z = k_z \frac{\partial p}{\partial z}$ and $u_r = k_r \frac{\partial p}{\partial r}$ are the velocity in transverse direction and radial direction, respectively. Figures 2–4 show the calculated normalized pressure profiles (top panels) and flow streamlines (bottom panels) for the membranes composed of two layers with different pore connectivity. It is assumed that a quarter of membrane area $\left(\frac{r_h}{r_c} = 0.5\right)$ is blocked by particles at the center of the characteristic region. Then, the corresponding normalized radial position r^* ranging from 0 to 1.0 represents the blocked regions. In these calculations, we assumed that the fouling layer is impermeable.

On the left side of Figure 2, the normalized permeability ratio K is equal to 1 in the upper layer (representing highly interconnected pores), whereas the normalized permeability ratio in the lower layer is equal to 0.1 (representing a layer of relatively lower pore connectivity). In contrast, the reverse arrangement was simulated on the right side of Figure 2, the normalized permeability ratio was varied from 0.1 to 1 piecewise from top to bottom. In this case, K is varied by changing k_r while keeping k_z constant. There is less pressure gradient in the upper layer for the membrane with higher pore connectivity than that with lower connectivity on the right panels. This is consistent with the idea that the interconnected pore structures can reduce the pressure difference between the open area and blocked area. As a result, the streamline starting from the brim of the blocked area goes farther in the radial direction in the upper layer for membrane with higher pore connectivity (left panels) on the top layer than that with lower connectivity on the right panels. Furthermore, the streamlines in the lower layer on the left side are almost straight lines because the lower layer has lower pore connectivity. In contrast to the left side, there is a significantly discontinuous inflection of streamlines on the right side. This indicates that the more interconnected pores in the lower layer will allow the fluid to flow underneath the top layer in the radial direction. Integrating the derivative of the pressure at the bottom of the membrane, we can get the normalized filtrate flux. For the case shown in the left panel, the normalized filtrate flux is 0.952, whereas the reversed arrangement on the right panels shows a normalized filtrate flux of 0.910. This indicates that although these two cases have two identical membranes oriented in different orders, the membrane with higher pore connectivity in the upper layer is more efficient in reducing the effect of the pore blockage, and gives a higher flux at equal extent of pore blockage. Thus, we predict that not only interconnectivity and asymmetry are important in fouling but also the order or direction of the asymmetry.

Next, we varied the normalized permeability ratio K (which represents the pore connectivity) by changing k_z but keeping the permeability in the radial direction k_r constant. This means that the membrane resistance will be changed in transverse direction. The pressure profiles and flow streamline were calculated and are shown in Figure 3 for

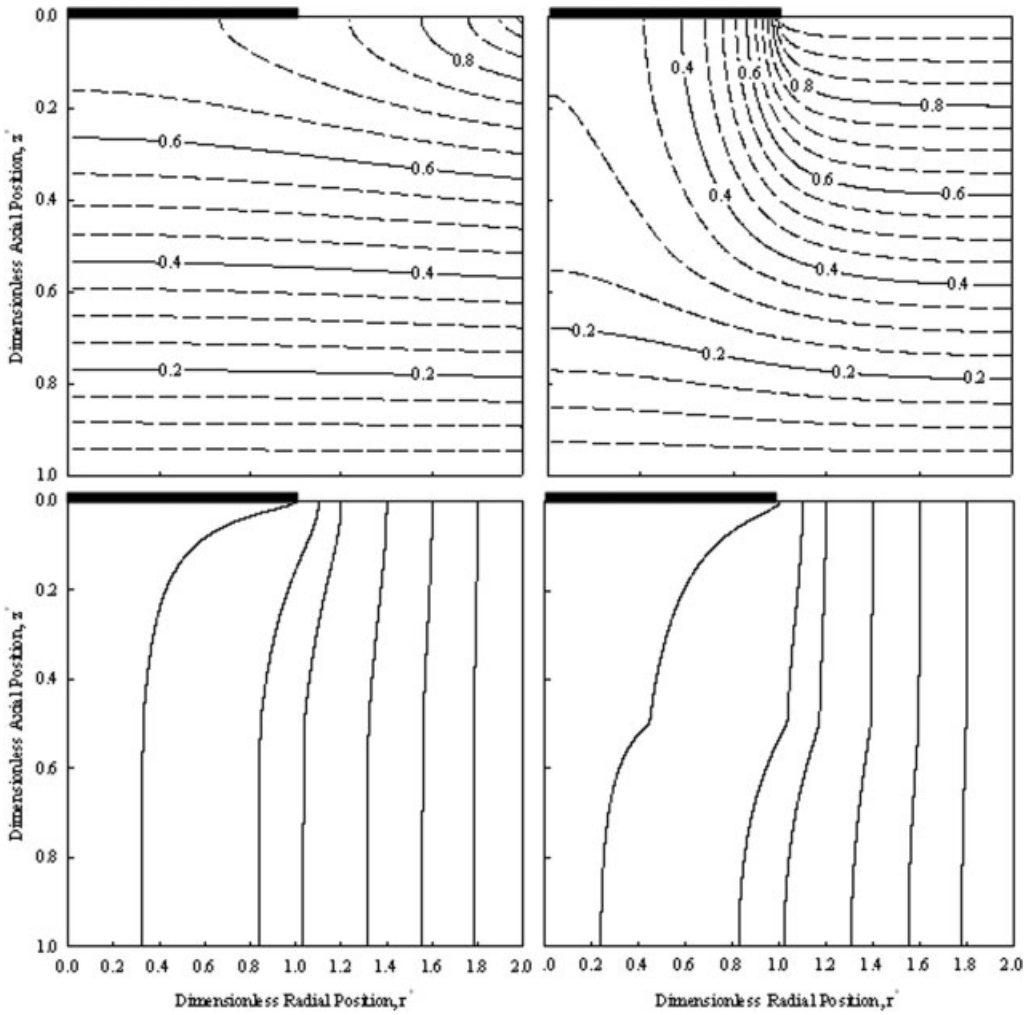

Figure 2. Normalized pressure profiles (top) and flow streamlines (bottom) within the membrane for membranes with the top half of the membrane having pore connectivity $K = 1$ and the bottom half of the membrane having $K = 0.1$ (left), the top half of the membrane having pore connectivity $K = 0.1$ and the bottom half of the membrane having $K = 1$ (right), while k_z is kept constant from top to bottom.

membranes with the normalized permeability ratio K varied from 1 to 0.1 (left panels) and 0.1 to 1 (right panels). The pressure gradient was concentrated within the layer of higher membrane resistance for both cases. In the left side, the normalized flux is 0.871. In the right side, the normalized flux is 0.938. It is interesting to note that although the left case has higher pore connectivity in the top layer, its normalized flux is lower than that of the right case of which top layer has lower pore connectivity. This indicates that the variation of membrane resistance in transverse direction can affect the normalized flux significantly. The model thus says that higher connectivity over lower connectivity is better when the connectivity is changed by altering k_r, but lower connectivity over higher connectivity is better when the connectivity is changed by altering k_z.

To study the effects of membrane resistance, we kept the normalized permeability ratio equal to one by increasing or decreasing both k_r and k_z on the same scale in the bottom half of the membrane. The calculation results were plotted in Figure 4. In the left side, both k_r and k_z were decreased 10 times in the bottom half of the membrane. This means that the bottom layer has higher membrane resistance than the top layer, and therefore the larger pressure gradient is located within the bottom layer as shown by the pressure profile plot. The normalized flux of the left side is 0.981. Conversely, in the right side both k_r and k_z were increased 10 times in the bottom half of the membrane, and the pressure gradient is much higher in the top layer. The normalized flux of the right side is 0.897. This value is significantly lower than the left side. This indicates that having higher membrane resistance in the bottom layer can enhance the normalized flux when the fouling all occurs at the top of the membrane.

To understand how these asymmetric structures affect the total filtrate flux, we calculated the normalized total filtrate flux as a function of the fraction of blocked area. The calculation results are plotted in Figure 5. When the normalized permeability ratio K is varied from 0.1 to 1 while keeping k_z constant, the normalized filtrate flux of the membrane with higher pore connectivity in the top layer is higher than that of the membrane with lower pore connectivity in the top

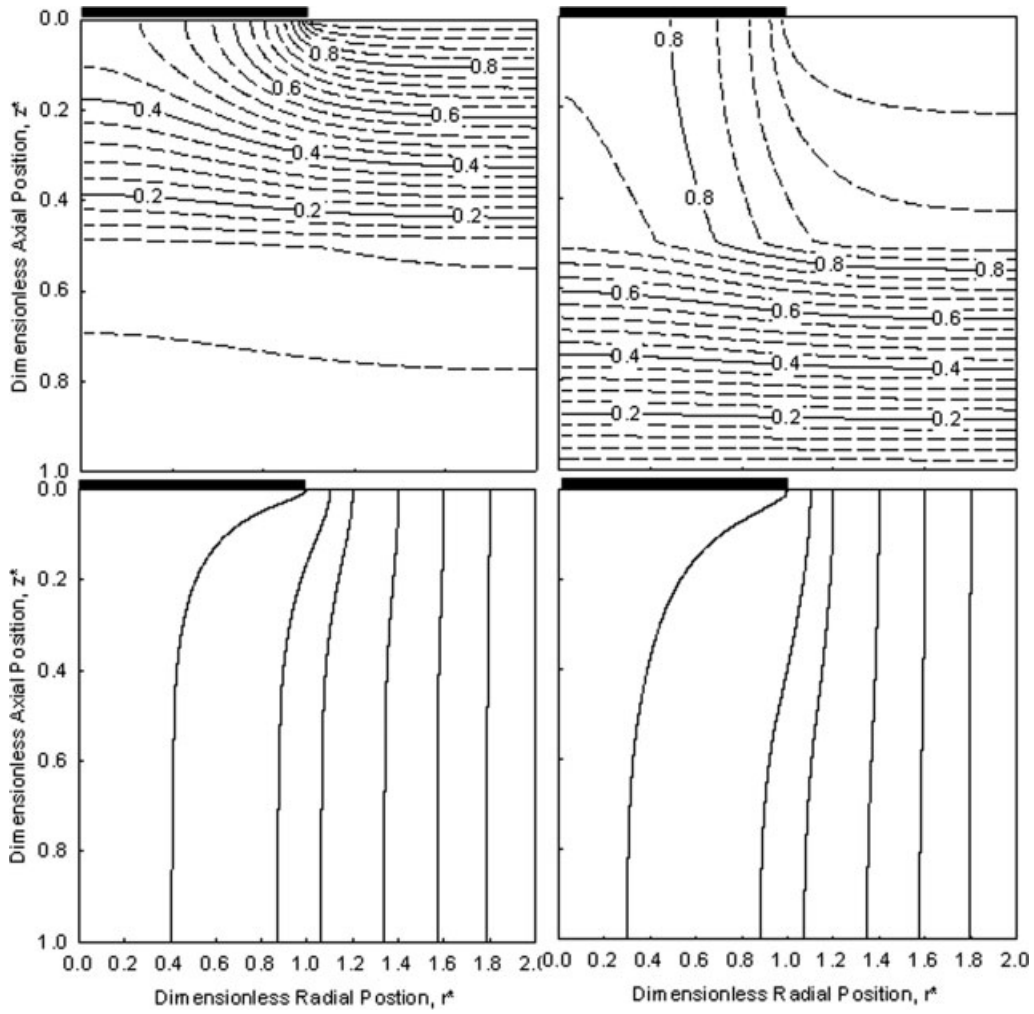

Figure 3. Normalized pressure profiles (top) and flow streamlines (bottom) within the membrane for membranes with the top half of the membrane having pore connectivity $K = 1$ and the bottom half of the membrane having $K = 0.1$ (left), the top half of the membrane having pore connectivity $K = 0.1$ and the bottom half of the membrane having $K = 1$ (right), while k_r is kept constant from top to bottom.

layer. However, when we varied the normalized permeability ratio in the same way while keeping k_r constant, the calculation results showed that the normalized flux of the membrane with higher pore connectivity in the top layer is lower than that of the membrane with lower pore connectivity in the top layer. When we set the permeability ratio equal to one, which represents higher pore connectivity, the membrane with the higher membrane resistance in the bottom layer has the highest normalized flux in all these cases. This indicates that the composite membrane with higher pore connectivity in the top layer and higher membrane resistance in the bottom layer has a higher normalized flux under the same extent of surface blockage.

Experimental Results and Model Validation

Model parameters

The external fouling parameters are necessary to validate this model accounting for membrane morphology. Because the fouling models assume that the membranes are composed of straight through noninterconnected pores, polycarbonate track-etched membranes (which have ideal uniform cylindrical pores) were used to obtain the external fouling parameters for pore blockage and cake filtration.

Solutions of 0.25 μm polystyrene microspheres, with concentrations from 0.000625 to 0.005 g/L, were filtered through 0.1 μm polycarbonate track-etched membranes under a constant pressure of 20 psi. The experimental results were plotted in Figure 6a. The initial filtrate flux ranged from 1.2×10^{-7} to 1.3×10^{-7} m^3/s. Based on the combined fouling model developed by Ho and Zydney,[4] the external fouling parameters, α for pore blockage and $f'R'$, R_{p0} for cake filtration, were fit using the experimental data from polycarbonate track-etched membranes. Best fit parameters are listed in Table 1. The solid curves in Figure 6 are model calculations using the best fit parameters shown in Table 1. Clearly, the fitting results are in good agreement with the experimental results across the entire range of microsphere concentrations.

Similarly, BSA solutions with concentration from 0.5 to 4 g/L were also filtered through 0.1 μm polycarbonate track-

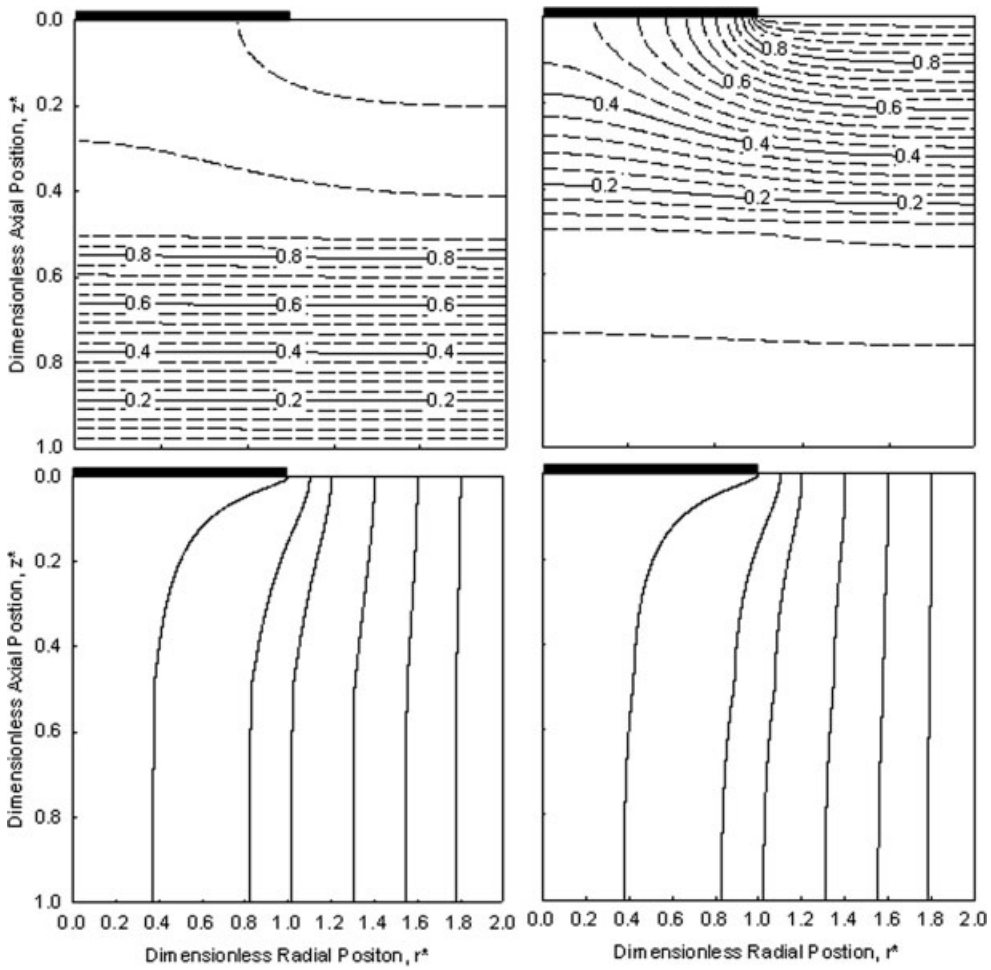

Figure 4. Normalized pressure profiles (top) and flow streamlines (bottom) within the membrane for membranes with both the top half and the bottom half of the membrane having pore connectivity $K = 1$, while both k_r and k_z are decreased 10 times (left), both k_r and k_z are increased 10 times (right).

etched membranes under a constant pressure of 20 psi. The experimental results were plotted in Figure 7a, and the best fit fouling parameters α, $f'R'$, and R_{p0} were also listed in Table 1.

Based on the fouling parameters from PCTE, the normalized permeability ratio K of Durapore membranes PVDF can be determined by filtration experiments. The solutions of 0.25 μm polystyrene microspheres with concentrations from 0.000625 to 0.005 g/L were filtered through 0.1 μm hydrophilic Durapore membranes under a constant pressure of 6 psi. The initial filtrate flux ranged from 1.2×10^{-7} to 1.3×10^{-7} m^3/s. Note that the 0.1 μm hydrophilic Durapore membranes were chosen to test the flux decline measurements other than 0.22 μm hydrophilic Durapore membranes. This is because the Durapore membranes have a distribution of pore size. 0.22 μm hydrophilic Durapore membranes are so close to the size of the polystyrene beads that this membrane may not be able to reject all beads. The experimental results were plotted in Figure 6b. The fouling model which accounts for the effects of membrane morphology on the flux decline, was used to calculate the curves. Comparing the model calculation with the experimental data to minimize the sum of the squared residuals, the best normalized

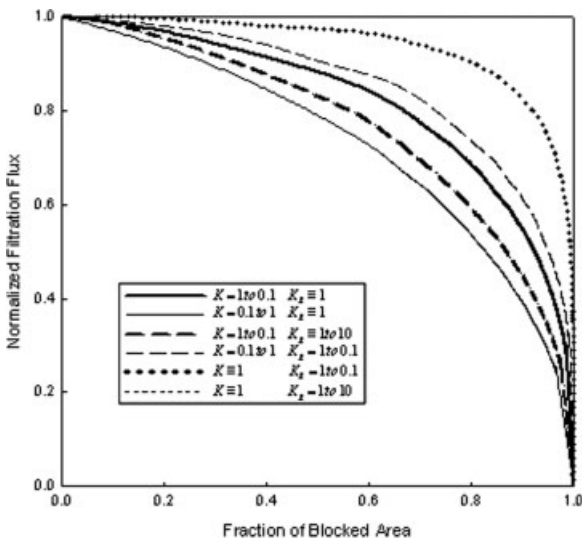

Figure 5. Normalized filtrate flux as a function of the fraction of blocked area for asymmetric composite membranes with the same total membrane resistance.

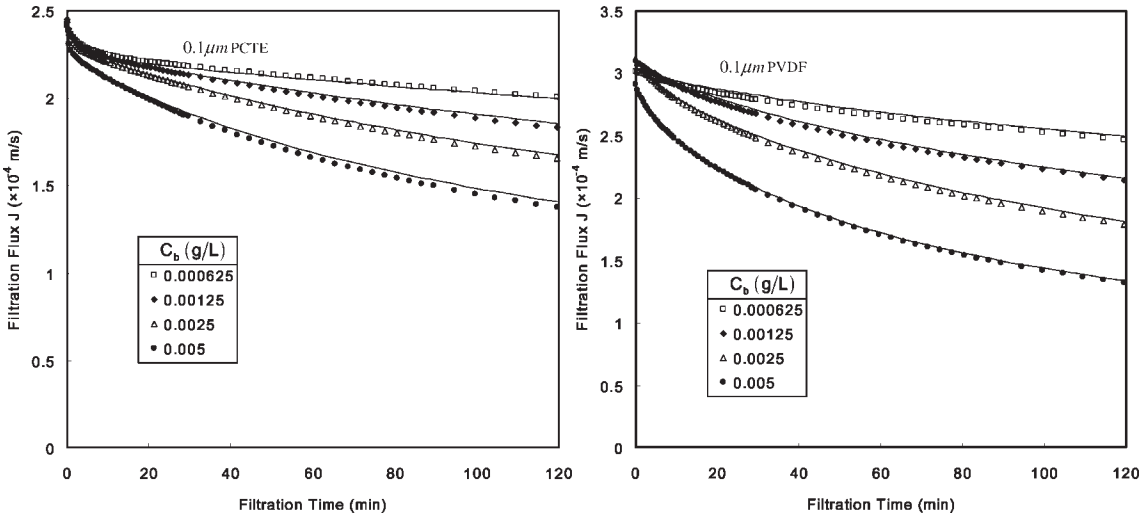

Figure 6. (a) 0.25 μm polystyrene beads filter through 0.1 μm PCTE, which has straight through pores, and the solid curves represent the model calculations based on combined fouling model; (b) 0.25 μm polystyrene beads filter through 0.1 μm PVDF, which has highly interconnectivity pores, and the solid curves represent the model calculations based on the fouling model accounting for the membrane morphology.

permeability ratio K of 0.1 μm Durapore membranes was determined as 0.90. The results of model calculation were plotted as solid curves in Figure 6b. There are two opposing factors that influence the flux decline behaviors of PCTE and Durapure membranes. First, the membrane resistance of 0.1 μm Durapore membranes is much lower than that of PCTE membranes, whereas the resistance of a single layer of 0.25 μm polystyrene beads is constant. As a result, the resistance ratio of a single layer of beads to a clean membrane is higher for the 0.1 μm Durapore membranes, and thus the normalized filtrate flux will be lower relative to the PCTE membranes. Second, the highly interconnected pores of Durapore membranes allow the fluid to flow around and under the blockage. For this reason, the total filtrate flux will be higher than the PCTE membrane.

BSA solutions were also filtered through 0.1 μm Durapore membranes to fit the best value of K. Both the experimental results and the model calculations were plotted in Figure 7b. The best value of K is 0.85, which is slightly lower than the value from polystyrene beads. This discrepancy is likely due to the particle size distribution of protein foulants, which is larger than that of polystyrene beads. Because of this, BSA solutions likely contain foulants that can block pores inside the membrane in addition to the top of the membrane.

Based on Eq. 15, the experimental data from the hydraulic permeability measurement of fouled PCTE membrane were plotted as $\ln(R_t - R_m - R_{p0})$ vs. $\ln(\Delta p)$ to fit the compressibility parameter S. The experimental results were plotted in Figure 8 for polystyrene bead (a) and BSA (b), respectively. Fitting results show that S is 0.37 ± 0.04 for BSA and 0.21 ± 0.03 for polystyrene bead. Note that the experimental value of S for polystyrene bead is not equal to zero, which is the theoretical value because polystyrene beads can be treated as rigid spheres. This is likely due to (1) tighter packing of polystyrene beads on membrane surface under higher pressures; or (2) stronger interaction between the beads and membrane surface caused by higher pressures.

Model validation

To validate the theoretical results of the composite membranes composed of two layers with different pore connectivity or membrane resistance, we formed asymmetric membrane by placing one membrane directly on top of another membrane having different pore connectivity or membrane resistance.

Figure 9 shows the flux decline data for 0.00125 g/L 0.25 μm polystyrene microspheres filtered through 0.2 μm PCTE, 0.1 μm PVDF, and the double-layer membranes composed of 0.1 μm PVDF and 0.2 μm PCTE. Pressure was adjusted to achieve the same initial flux 3×10^{-4} m/s. The composite membrane with the PVDF on the top of PCTE has a higher filtrate flux than the composite membrane with the inverse arrangement. Each layer of the composite membrane was tested for hydraulic permeability before and after the flux decline measurements. Figure 9b shows the ratio of initial permeability and final permeability for both the top and bottom layer. The permeability of the bottom layer remains more than 90% of the initial value after the filtration. This indicates that external fouling is the dominant mechanism during the filtration processes with most of the fouling occurring at the top layer regardless of the membrane used in the top layer.

Figure 10 shows the flux decline data for 0.00125 g/L 0.25 μm polystyrene microspheres filtering through 0.1 μm

Table 1. Best Fit Parameters for PCTE Membranes

Solutions	α (m^2/kg)	$f'R'$ (m/kg)	R_{p0} (m^{-1})
PS bead	$1.57 \pm 0.1 \times 10^4$	$3.79 \pm 0.1 \times 10^{13}$	$1.81 \pm 0.2 \times 10^{10}$
BSA	6.34 ± 0.2	$4.20 \pm 0.1 \times 10^{11}$	$1.59 \pm 0.3 \times 10^{10}$

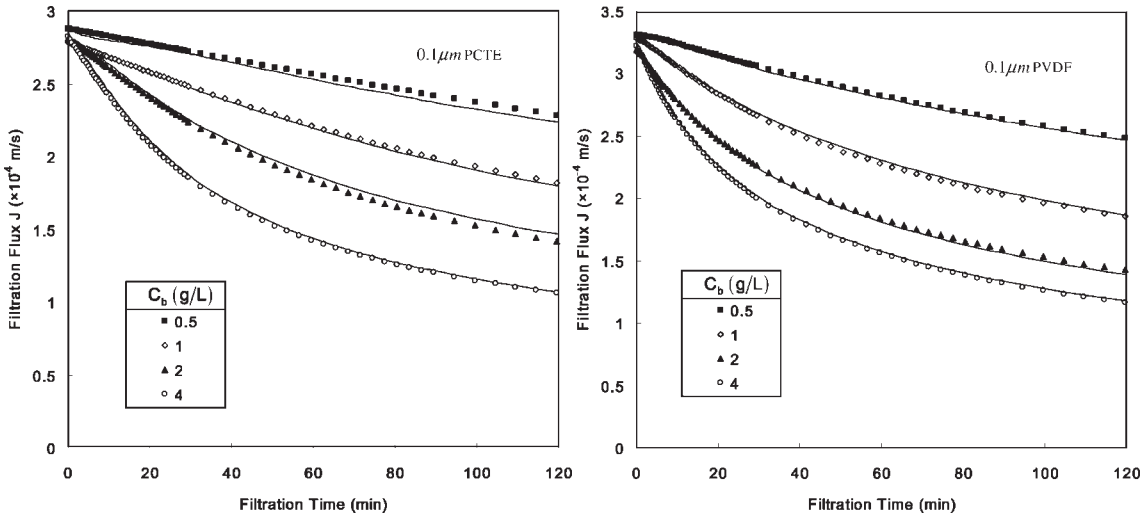

Figure 7. (a) BSA solutions filter through 0.1 μm PCTE, which has straight through pores, and the solid curves represent the model calculations based on combined fouling model; (b) BSA solutions filter through 0.1 μm PVDF, which has highly interconnectivity pores, and the solid curves represent the model calculations based on the fouling model accounting for the membrane morphology.

PVDF, and the double-layer membranes with 0.1 μm PVDF in the top layer while the nominal pore size of PVDF was varied from 0.1 to 0.45 μm. Pressure was varied from 6 to 12 psi correspondingly to keep the same initial flux of 3×10^{-4} m/s. The filtrate flux increases with increasing membrane resistance of the bottom layer. This is consistent with the theoretical analysis. The results of permeability test for each layer of the composite membranes are plotted in Figure 10b, and the dominance of external fouling was validated.

The fouling model accounting for the effects of membrane morphology was applied to the prediction of the flux decline. The results of model calculation (based on the parameters listed in Tables 2 and 3) are presented as solid curves in Figures 9a and 10a. Note that the best fit parameters (K) are different for single layer and composite membranes. This is due to the higher thickness of the composite membrane. As shown in Eq. 10, K is proportional to δ_m^2. The compressibility parameter S was set to 0.19 for calibrating specific cake layer resistance R' when the transmembrane pressure was larger than 2 psi. All the experimental results were consistent with the model predictions, indicating that a composite membrane with higher pore connectivity on the top layer and higher membrane resistance in the bottom layer is the optimum configuration of the options tested here.

Similarly, the same flux decline measurements were done using BSA. Figure 11 shows the flux decline for 1 g/L BSA solutions filtering through 0.2 μm PCTE, 0.1 μm PVDF, and the composite membranes composed of 0.2 μm PCTE and 0.1 μm PVDF in different order. Pressure was varied from 2 to 8 psi correspondingly to keep the same initial flux of 3×10^{-4} m/s. The composite membrane with 0.1 μm PVDF on the top of 0.2 μm PCTE is better than the composite

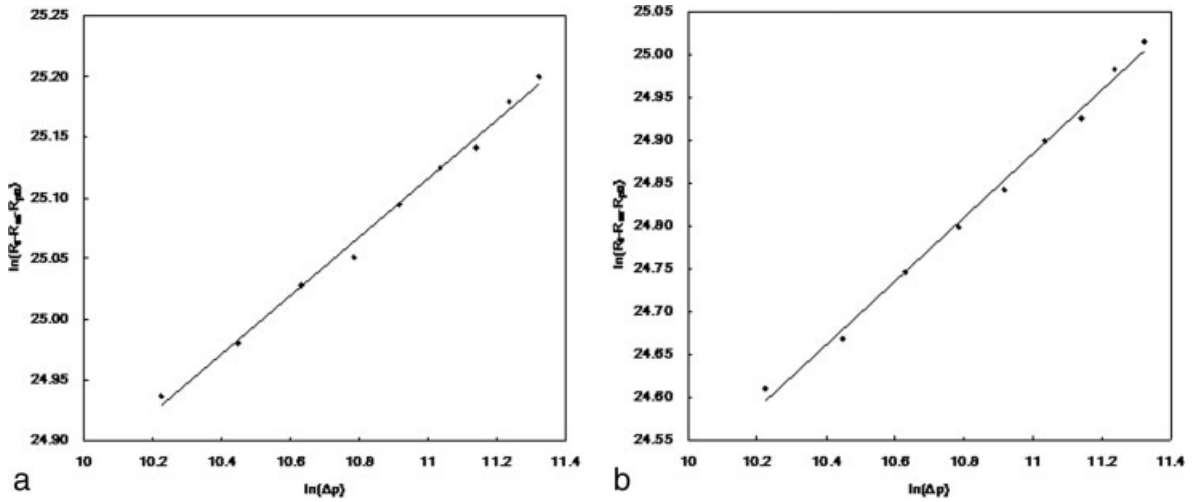

Figure 8. (a) Experimental data fitting of compressibility parameter S based on Eq. 15 for polystyrene bead; (b) experimental data fitting of compressibility parameter S based on Eq. 15 for BSA.

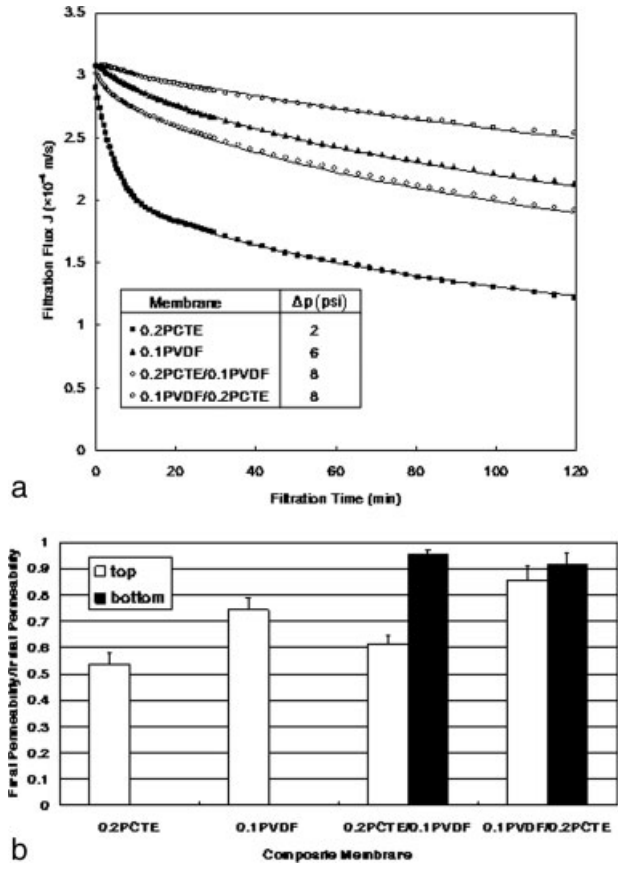

Figure 9. (a) Flux decline data for 0.25 μm polystyrene microsphere solutions through the double-layer membranes with 0.1 μm hydrophilic Durapore membranes on the top of 0.2 μm polycarbonate track-etched membranes or the inverse arrangement.

Solid curves are model calculations based on the best fitting parameters listed in Table 2. (b) The ratio of permeability before and after filtration.

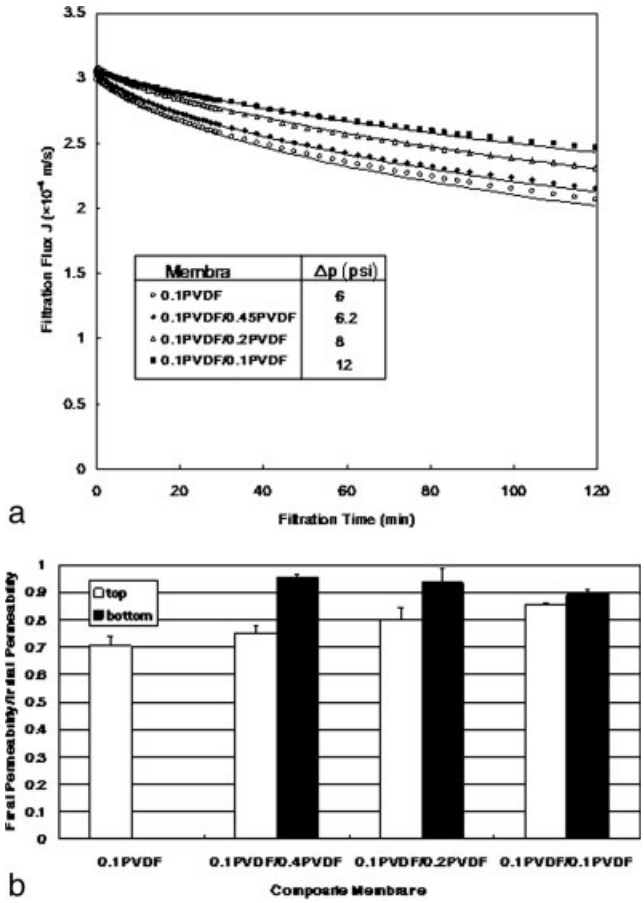

Figure 10. (a) Flux decline data for 0.25 μm polystyrene microsphere solutions through the double-layer membranes with 0.1 μm hydrophilic Durapore membranes on the top of hydrophilic Durapore membranes of which pore size varies from 0.1 to 0.45 μm.

Solid curves are model calculations based on the best fitting parameters listed in Table 3. (b) The ratio of permeability before and after filtration.

membrane with 0.2 μm PCTE on the top of 0.1 μm PVDF because of the highly interconnected structures on the top layer. The results of permeability test before and after filtration, plotted in Figure 11b, show the ratio of initial permeability and final permeability is still above 85% for the bottom layers. This indicates that external fouling is still dominant during the filtration of protein solutions.

Figure 12 shows the flux decline data for 1 g/L BSA filtering through 0.1 μm PVDF, and the double-layer membranes with 0.1 μm PVDF in the top layer while the nominal pore size of the bottom layer was varied from 0.1 to 0.45 μm. Pressure was varied from 6 to 12 psi correspondingly to keep the same initial flux of 3×10^{-4} m/s. The corresponding experimental results of the hydraulic permeability test before and after filtration were plotted in Figure 12b. When increasing the membrane resistance of the bottom layer, the fouling was reduced as shown in Figure 12a.

Based on the fouling parameters listed in Tables 4 and 5, the corresponding flux decline of BSA through different

Table 2. Parameters of Model Calculations for PS Bead (1)

	0.2 PCTE	0.1 PVDF	0.2 PCTE/0.1 PVDF	0.1 PVDF/0.2 PCTE
α' (m^2/kg)	$5.71 \pm 0.2 \times 10^3$	$5.71 \pm 0.2 \times 10^3$	$5.71 \pm 0.2 \times 10^3$	$5.71 \pm 0.2 \times 10^3$
$f'R'$ (m/kg)	$3.79 \pm 0.1 \times 10^{13}$	$4.67 \pm 0.1 \times 10^{13}$	$4.93 \pm 0.1 \times 10^{13}$	$4.93 \pm 0.1 \times 10^{13}$
R_{p0} (m^{-1})	$1.81 \pm 0.2 \times 10^{10}$	$1.81 \pm 0.2 \times 10^{10}$	$1.81 \pm 0.2 \times 10^{10}$	$1.81 \pm 0.2 \times 10^{10}$
K (top)	0	0.93	0	1.29
K (bottom)			1.29	0

Table 3. Parameters of Model Calculations for PS Bead (2)

	0.1 PVDF	0.1 PVDF/0.45 PVDF	0.1 PVDF/0.22 PVDF	0.1 PVDF/0.1 PVDF
α' (m^2/kg)	$5.71 \pm 0.2 \times 10^3$	$5.71 \pm 0.2 \times 10^3$	$5.71 \pm 0.2 \times 10^3$	$5.71 \pm 0.2 \times 10^3$
$f'R'$ (m/kg)	$4.67 \pm 0.1 \times 10^{13}$	$4.70 \pm 0.1 \times 10^{13}$	$4.93 \pm 0.1 \times 10^{13}$	$5.33 \pm 0.1 \times 10^{13}$
R_{p0} (m^{-1})	$1.81 \pm 0.2 \times 10^{10}$	$1.81 \pm 0.2 \times 10^{10}$	$1.81 \pm 0.2 \times 10^{10}$	$1.81 \pm 0.2 \times 10^{10}$
K (top)	0.93	3.72	3.72	3.72
K (bottom)		3.72	3.72	3.72

composite membranes was predicted by the fouling model accounting for the membrane morphology. The compressibility parameter S was set to 0.40 for calibrating specific cake layer resistance R' when the transmembrane pressure was larger than 2 psi. The model calculation results were plotted in Figures 11a and 12a as solid curves. Experimental results are consistent with the model prediction. The composite membrane with higher pore connectivity on the top layer and higher membrane resistance in the bottom layer can reduce the fouling caused by protein aggregates.

To compare the performance of the various asymmetric membrane structures, we calculated the volumetric filtrate flux at 2 h after filtering 1 g/L BSA solutions to examine the productivity at this particular time point. The system capacity was assumed to be the volume of filtrate processed until the flux dropped to 10% of the initial value at time t_p, and calculated by:

$$\text{Capacity} = \int_o^{t_p} J(t)dt. \tag{22}$$

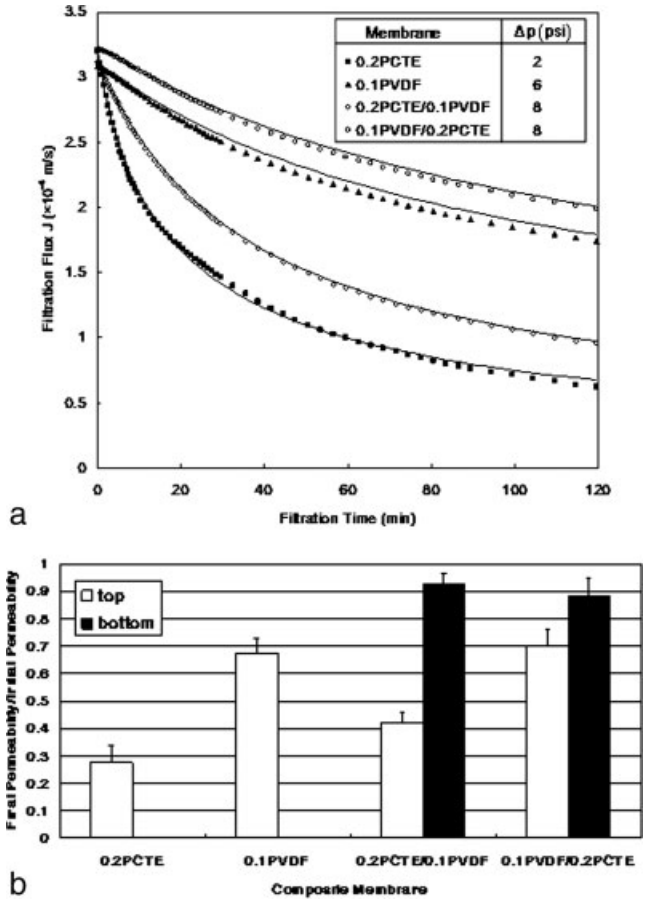

Figure 11. (a) Flux decline data for BSA solutions through the double-layer membranes with 0.1 μm hydrophilic Durapore membranes on the top of 0.2 μm polycarbonate track-etched membranes or the inverse arrangement.

Solid curves are model calculations based on the best fitting parameters listed in Table 4. (b) The ratio of permeability before and after filtration.

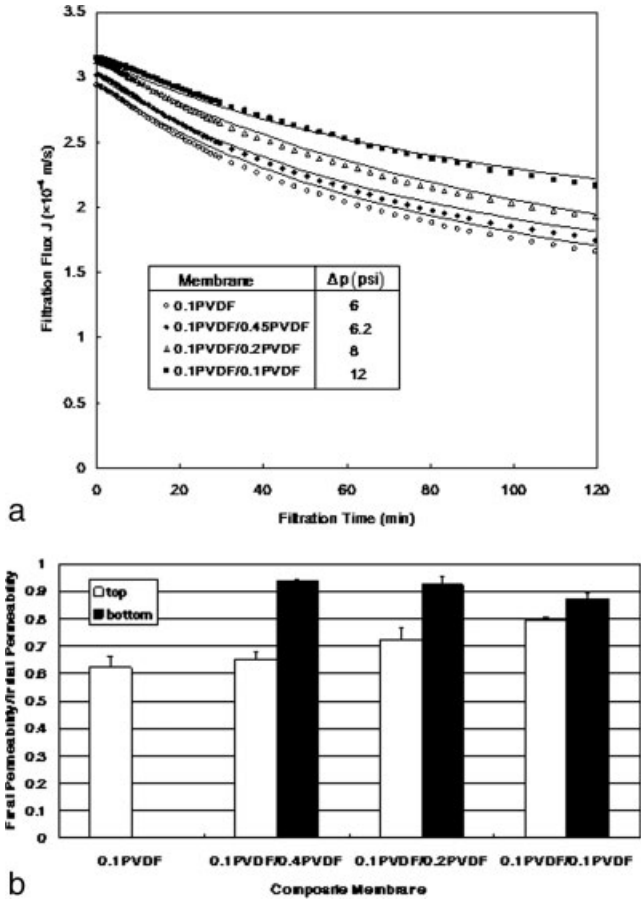

Figure 12. (a) Flux decline data for BSA solutions through the double-layer membranes with 0.1 μm hydrophilic Durapore membranes on the top of hydrophilic Durapore membranes of which pore size varies from 0.1 to 0.45 μm.

Solid curves are model calculations based on the best fitting parameters listed in Table 5. (b) The ratio of permeability before and after filtration.

Table 4. Parameters of Model Calculations for BSA (1)

	0.2 PCTE	0.1 PVDF	0.2 PCTE/0.1 PVDF	0.1 PVDF/0.2 PCTE
α' (m^2/kg)	1.35 ± 0.2	1.35 ± 0.2	1.35 ± 0.2	1.35 ± 0.2
$f'R'$ (m/kg)	$4.20 \pm 0.1 \times 10^{11}$	$6.52 \pm 0.1 \times 10^{11}$	$7.31 \pm 0.1 \times 10^{11}$	$7.31 \pm 0.1 \times 10^{11}$
R_{p0} (m^{-1})	$5.14 \pm 0.3 \times 10^{10}$	$5.14 \pm 0.3 \times 10^{10}$	$5.14 \pm 0.3 \times 10^{10}$	$5.14 \pm 0.3 \times 10^{10}$
K (top)	0	0.86	0	1.19
K (bottom)			1.19	0

Table 5. Parameters of Model Calculations for BSA (2)

	0.1 PVDF	0.1 PVDF/0.45 PVDF	0.1 PVDF/0.22 PVDF	0.1 PVDF/0.1 PVDF
α' (m^2/kg)	1.35 ± 0.2	1.35 ± 0.2	1.35 ± 0.2	1.35 ± 0.2
$f'R'$ (m/kg)	$6.52 \pm 0.1 \times 10^{11}$	$6.55 \pm 0.1 \times 10^{11}$	$7.31 \pm 0.1 \times 10^{11}$	$8.60 \pm 0.1 \times 10^{11}$
R_{p0} (m^{-1})	$5.14 \pm 0.3 \times 10^{10}$	$5.14 \pm 0.3 \times 10^{10}$	$5.14 \pm 0.3 \times 10^{10}$	$5.14 \pm 0.3 \times 10^{10}$
K (top)	0.86	3.44	3.44	3.44
K (bottom)		3.44	3.44	3.44

All calculations were based on the parameters listed in Tables 3 and 4. The calculation results were listed in Table 6. It shows that both the instant productivity and capacity of the composite membrane 0.1 μm PVDF/0.1 μm PVDF are higher than that for the single 0.1 μm PVDF membrane. For 0.2 μm PCTE and 0.1 μm PVDF membranes, the productivity at 2 h is higher for 0.1 μm PVDF/0.2 μm PCTE. The system capacity for 0.1 μm PVDF/0.1 μm PVDF is the highest, which nearly doubled than that for the single 0.1 μm PVDF. The results indicate that composite membranes can have better productivity and capacity than single-layer membranes.

Conclusions

A mathematical model accounting for the effects of asymmetric membrane structure on the fouling processes has been developed. The permeability ratio describing the pore interconnectivity and membrane resistance was varied in the transverse direction piecewise to simulate the different asymmetric structures of composite membranes. Model calculations were plotted as normalized pressure profiles and flow streamlines. Using a combined pore blockage and cake filtration model, the flux decline profiles of different asymmetric structures were studied. The results of theoretical analysis show that composite membranes with higher pore interconnectivity in the upper layer and higher membrane resistance in the lower layer can more efficiently minimize flux decline during the filtration.

Based on the fouling parameters and permeability ratio, which were determined by filtration experiments of single-layer symmetric membranes, the model predictions were compared with the experimental results of double-layer membranes with (1) 0.1 μm PVDF on the top of 0.2 μm PCTE or the inverse arrangement, (2) 0.1 μm PVDF on the top layer with the bottom layer pore size varied from 0.1 to 0.45 μm (all PVDF). The model predictions for the flux decline for the composite membranes with parameters obtained from fitting the experimental data of single-layer membranes were in good agreement with the experimental results.

Table 6. Instant Productivity and Capacity for BSA (1 g/L)

Membrane Combination	Instant Productivity after 2 h ($\times 10^{-8} m^3/s$)	Capacity (m^3/m^2)
0.2 PCTE	2.65	2.61
0.1 PVDF	6.98	16.90
0.2 PCTE/0.1 PVDF	3.78	6.66
0.1 PVDF/0.2 PCTE	7.84	21.55
0.1 PVDF/0.45 PVDF	7.10	17.88
0.1 PVDF/0.22 PVDF	7.60	22.11
0.1 PVDF/0.1 PVDF	8.66	32.76

All these studies indicate that composite membranes with higher pore interconnectivity in the upper layer and higher membrane resistance in the lower layer are better than the others providing that the dominant fouling mechanism is external fouling. This optimized morphology has the potential to help to design new membranes with better fouling resistance.

In this study, we used pure polystyrene microsphere solution and/or pure BSA solution as a model system. For most actual processes, the real feed usually contains whole cells, proteins, and cell debris. To extend this work to more complex feed, more studies need to be done to relate the feed stream content to the fouling parameters, such as α, R', and R_{p0}. In the future study, we will present how to obtain the fouling parameters based on the size and amount of the foulant, pore size of the membranes, and the porosity of the cake layer.

Acknowledgements

The support of National Science Foundation Center for Membrane Applied Science and Technology (MAST) and Millipore Corporation is highly appreciated.

Notation

A_u = area of unblocked membrane m^2
C_b = bulk concentration g/L
f' = fraction of particle contributing to cake layer
J_b = flux within the blocked region m/s
J_u = flux within the unblocked region m/s
k_r = Darcy permeability in radial direction m^3 s/kg
k_z = Darcy permeability in axial direction m^3 s/kg
k_p = proportionality coefficient for cake layer resistance m/kg
K = normalized permeability ratio $k_r\delta_m{}^2/k_z r_c{}^2$
K_z = dimensionless permeability in axial direction $k_z/k_z|_{z=0}$
p = pressure N/m^2
p_f = feed stream pressure N/m^2

p_p = permeate stream pressure N/m^2
r = radial coordinate m
r_b = radius of blocked region (left panel in Figure 1) m
r_c = radius of the flow cylinder (Figure 1) m
r_m = radius of membrane pores m
r_p = radius of particles m
r_u = radius of unblocked region (right panel in Figure 1) m
r^* = normalized radial coordinate r/r_c
R_p = resistance of cake layer m^{-1}
R' = specific cake layer resistance m/kg
S = compressibility coefficient for cake layer
t = filtration time s
u_r = radial velocity m/s
u_z = axial velocity m/s
z = axial coordinate m
z^* = normalized axial coordinate z/δ_m
α = area of blocked membrane per unit particle mass m^2/kg
α' = area of particle per unit particle mass m^2/kg
δ_m = thickness of membrane m
ε_m = porosity of membrane
μ = viscosity of solution Pa s
θ = fraction of blocked membrane area
ψ = stream function m^3/s

Literature Cited

1. Suki A, Fane AG, Fell CJD. Flux decline in protein ultrafiltration. *J Membr Sci*. 1984;21:269–283.
2. Bowen WR, Gan Q. Properties of microfiltration membranes: the effects of adsorption and shear on the recovery of an enzyme. *Biotechnol Bioeng*. 1992;40:491–497.
3. Tracey EM, Davis RH. Protein fouling of track-etched polycarbonate microfiltration membranes. *J Colloid Interface Sci*. 1994;167:104–116.
4. Ho CC, Zydney AL. A combined pore blockage and cake filtration model for protein fouling during microfiltration. *J Colloid Interface Sci*. 2000;232:389–399.
5. Duclos-Orsello C, Li WY, Ho CC. A three mechanism model to describe fouling of microfiltration membranes. *J Membr Sci*. 2006; 280:856–866.
6. Bolton G, LaCasse D, Kuriyel R. Combined models of membrane fouling: development and application to microfiltration and ultrafiltration of biological fluids. *J Membr Sci*. 2006;277:75–84.
7. Ho CC, Zydney AL. Effect of membrane morphology on the initial rate of protein fouling during microfiltration. *J Membr Sci*. 1999; 155:261–275.
8. Ho CC, Zydney AL. Theoretical analysis of the effect of membrane morphology on fouling during microfiltration. *Sep Sci Technol*. 1999;34:2461–2483.
9. Ho CC, Zydney AL. Measurement of membrane pore interconnectivity. *J Membr Sci*. 2000;170:101–112.
10. Jackson NM, Jafferali R, Bell DJ, Davies GA. A study of the structure of micro and ultra filtration membranes: the Voronoi tessellation as a stochastic model to simulate the structure. *J Membr Sci*. 1999; 162:23–43.
11. Matsuyama H, Teramoto M, Uesaka T. Membrane formation and structure development by dry-cast process. *J Membr Sci*. 1997;135: 271–288.
12. Albrecht W, Kneifel K, Weigel Th, Hilke R, Just R, Schossig M, Ebert K, Lendlein A. Preparation of highly asymmetric hollow fiber membranes from poly(ether imide) by a modified dry-wet phase inversion technique using a triple spinneret. *J Membr Sci*. 2005;262: 69–80.
13. Pradanos P, Hernandex A, Calvo JI, Tejerina F. Mechanisms of protein fouling in cross-flow UF through an asymmetric inorganic membrane. *J Membr Sci*. 1996;114:115–126.
14. Fomovska GN, Pesci SE. Isotropic glass fiber media versus asymmetric BTS SP300 membranes for plasma separation from whole blood. *Clin Chem*. 2004;50 (Part 2):A31–A31.
15. Kools W. Process of forming multilayered structures. US Patent No 7. 2007; 208:200.
16. Ho CC, Zydney AL. Protein fouling of asymmetric and composite microfiltration membranes. *Ind Eng Chem Res*. 2001;40:1412–1421.
17. Zydney AL, Ho CC. Effect of membrane morphology on system capacity during normal flow microfiltration. *Biotechnol Bioeng*. 2003;83:537–543.
18. Krogh A. The supply of oxygen to the tissues and the regulation of the capillary circulation. *J Physiol*. 1918;52:457.
19. Ho CC, Zydney AL. Transmembrane pressure profiles during constant flux microfiltration of bovine serum albumin. *J Membr Sci*. 2002;209:363–377.
20. Griffiths DV, Smith IM. *Numerical Methods for Engineers*. Boca Raton, FL: Chapman and Hall/CRC, 2006.

Manuscript received Jan. 17, 2008, and revision received Nov. 6, 2008.